




Flexible piezoelectric nanogenerator based on [P(VDF-HFP)]/ PANI-ZnS electrospun nanofibers for electrical energy harvesting

Hemalatha Parangusan¹, Jolly Bhadra¹ , and Noora Al-Thani^{1,*}

¹ Young Scientist Center (YSC), Qatar University, P.O. Box 2713, Doha, Qatar

Received: 26 September 2020

Accepted: 15 January 2021

Published online:
19 February 2021

© The Author(s) 2021

ABSTRACT

Over the past decade, piezoelectric nanogenerator have attracted much attention to harvest mechanical energy from abundant resources in nature. Here, the ZnS microspheres is prepared by hydrothermal method and core-shell structured PANI/ZnS microspheres are synthesized by in situ polymerization method and then used as filler for the preparation of flexible [P(VDF-HFP)] based piezoelectric nanogenerator. The flexible P(VDF-HFP)/PANI-ZnS piezoelectric nanogenerator is prepared by Electrospinning technique. The core-shell PANI/ZnS composite improves the content of electroactive phase in [P(VDF-HFP)] and significantly improves the interfacial polarization between the PANI/ZnS particles and polymer matrix. Among all the samples, [P(VDF-HFP)]/2 wt% PANI-ZnS composite nanofibers exhibited the high piezoelectric peak-to-peak output voltage of 3 V compared with the neat [P(VDF-HFP)] (~ 120 mV). In addition, the high dielectric constant is observed for the [P(VDF-HFP)]/2 wt% PANI-ZnS composite nanofibers. These results implies that the fabricated flexible and efficient piezoelectric nanogenerator can be utilized for energy harvesting system.

1 Introduction

Due to the growing population and the rising demand for energy have motivated the development of few alternative power sources [1]. However, several kinds of alternative energy sources such as solar energy, supercapacitor and Li-ion battery have been developed. Among them mechanical energy is very attractive for harvesting energy due to its availability

in nature [2]. Recently, piezoelectric nanogenerator (NG) is a promising technology for harvesting mechanical energy because of their ability to convert the mechanical energy to electric energy by means of a piezoelectric material. When the external mechanical force is applied, these materials accumulate electrical charges. Piezoelectric or ceramic materials, such as ZnO nanowires, BaTiO₃ thin films, lead zirconium titanate (PZT), Zinc sulphide (ZnS) and lithium niobate have been used for the assembly of piezoelectric

Address correspondence to E-mail: n.al-thani@qu.edu.qa

nanogenerator. However, their brittle nature causes limitation in the wearable and flexible technology applications, especially in the bulk form [3–5]. Recently, Poly(vinylidene difluoride) (PVDF) and its copolymers poly(vinylidene fluoride-trifluoroethylene) [P(VDF-TrFE)] and poly(vinylidene fluoride-hexafluoropropylene) [P(VDF-HFP)] finding interesting applications in actuators, sensors, energy harvesting and in the biomedical applications [6]. This is due to their flexibility, lightweight and environmental compatibility.

The combination of the piezoceramic and piezoelectric polymers improve the thermal, mechanical and barrier properties due to the addition of filler in a polymer matrix [7]. Among the various available piezoelectric materials, the noncentrosymmetric ZnS has gained much attention and used in flat panel displays, luminescent devices, sensors and lasers, infrared windows [8–10]. In addition, ZnS is a biocompatible and nontoxic material with higher piezoelectric properties, but it is not as widely researched as ZnO, lead zirconium titanate and Barium titanate in piezotronic devices. The ZnS also have excellent acoustoelectric properties and optical conductivity and thus can be used in diverse applications. It has been reported that the polymer nanocomposites are limited by the internal resistance and relatively low short-circuit current [11]. Recently, conductive fillers such as graphene, polyaniline (PANI) and Carbon nanotube (CNT) has gained tremendous interest of researchers [12]. These fillers reduces the internal resistance of nanogenerator and easily forms conduction pathway by its network structure [13]. In addition, the incorporation of nanofillers leads to the enhancement of the β -crystalline phase of PVDF, which contributes to the increase in energy harvesting performance of the nanocomposites. Mokhtari et al. [14] developed piezoelectric nanogenerator based on PVDF containing different additives (ZnO, CNT, LiCl, PANI). They compared β -phase formation with different additives and found that the fillers are important for the β -phase formation.

Several research groups widely used the “poling” procedure for higher β - phase nucleation, which is attained by the application of electric field under mechanical stretching. One of the promising alternatives in this regard is the self-polarized piezoelectric nanogenerator. Recently, researchers reported the electrospun nanofibers as an energy harvesting

devices because the nanofibers could be assembled as piezoelectric nanogenerator directly without any poling treatments. Li et al. have fabricated piezoelectric membrane device by using electrospinning method. They have reported that the fabricated device exhibits high open-circuit voltage, power density, short-circuit current and electric output [15]. Persano et al. have prepared [P(VDF-TrFe)] nanofibers by electrospinning method. This method is suitable for producing self-poled piezoelectric nanofibers [16].

In the present work, PANI coated ZnS microspheres have been synthesized by hydrothermal and in situ-polymerization method before its addition into [P(VDF-HFP)]. The incorporation of conducting polyaniline as a filler into [P(VDF-HFP)] nanofibers. ZnS acted as a nucleating agent and the conducting filler act as dispersant, energy enhancer and conducting functional materials in PVDF matrix. The present work also emphasizes the suitability of PANI coated ZnS microspheres for the preparation of [P(VDF-HFP)] nanofibers for energy harvesting applications.

2 Experimental

Poly(vinylidene fluoride-hexafluoropropylene) ($M_w = 400,000$), Acetone and N,N dimethylformamide (DMF) are obtained from sigma Aldrich. Aniline, APS (Ammonium per sulphate) and HCl are used for the preparation of PANI and Zinc acetate dehydrate, thiourea, polyethylene glycol (PEG) are purchased for the synthesis of ZnS. All the chemicals are obtained from sigma Aldrich.

2.1 Preparation of ZnS microsphere

Hydrothermal method is used to synthesize the ZnS microspheres. Initially, required amount of Zinc acetate dehydrate is dissolved in 50 ml distilled water. Then 0.5 g PEG surfactant is added to this solution. Next, 1 g thiourea is added to the above solution. The final solution is transferred to Teflon-lined autoclave of 100 mL capacity and then subjected to heat at 160 °C for 3 h. After the complete reaction process, the Teflon-lined autoclave is cooled down to room temperature. The white precipitates are collected and rinsed several times with distilled water and ethanol, subsequently for several times

and then the resultant precipitates are dried in a vacuum oven at 60 °C .

2.2 Synthesis of PANI coated ZnS microspheres

The typical preparation procedure of PANI-ZnS composites is as follow: 0.2 M aniline and 3 wt% percentage ZnS microspheres are dispersed into 50 mL of 0.01 M HCL solution and the mixture is stirred in an ice-bath for 2 h. In this solution, ammonium persulfate (0.2 M) is added drop wise with continuous stirring for overnight, APS acts as the oxidant. Subsequently, the precipitate powder is filtered and rinsed with distilled water and ethanol. Finally, the precipitate is dried at 60 °C in a vacuum oven.

2.3 Fabrication of P(VDF-HFP)/PANI-ZnS composite electrospun nanofibers

First, an appropriate amount of [P(VDF-HFP)] is dissolved in the N, N dimethylformamide (DMF) and Acetone mixture (ratio of DMF and Acetone ~ 1:1) under stirring for 3 hrs at 70 °C. Subsequently, 2 wt% of PANI coated ZnS microspheres is dispersed in the DMF and Acetone mixture by sonication for 2 h. Finally, the PANI coated ZnS microspheres solution is mixed with [P(VDF-HFP)] solutions. Then the resultant solution is kept for overnight stirring. The electrospinning process is started by loading the [P(VDF-HFP)]/2 wt% PANI-ZnS solution into a 20 mL plastic syringe. The distance between the collector and the needle is 12 cm and the applied voltage is 12 kV. A constant flow rate (1.2 ml/h) of the polymer solution is applied throughout the fiber collection process. The electrospinning experiment is carried out at a temperature of 23 °C and a relative humidity of 30 %. The same procedure is followed for the [P(VDF-HFP)]/ZnS and [P(VDF-HFP)]/PANI nanocomposites. The obtained samples are labeled as PHP, P-PANI, P-ZnS and P-PANI-ZnS.

2.4 Characterization

The phase and crystalline nature of the composites are examined by using Empyrean X-ray powder diffractometer, Panalytical model, UK. The morphologies of the products are observed by using Scanning electron microscope (SEM) (Nova Nano

SEM 450) and Transmission electron microscope (TEM) (Phillips CM 12). The dielectric properties of electrospun nanofibers are measured using a GMbH concept 40 (NOVO control Technologies, Germany). The universal testing machine (Lloyd IKN LF Plus, AMETEK, Inc., Bognor Regis, UK) at 5 mm/min is used to obtain the stress-strain curve. Piezoelectric testing system is similar to our previous report [17]. The output voltage from the piezoelectric nanogenerator is measured using a combination of vibrating shaker, amplifier, frequency generator, and resistor box and data acquisition system. The sample is placed on the vibrating shaker with the mass of 2.5 N and causing a compressive force. The electrical output is measured by a data acquisition system.

3 Results and discussion

A schematic representation of the fabrication of composite electrospun nanofibers are shown in Fig. 1. The PANI coated ZnS microsphere are prepared by hydrothermal and in situ polymerization method as represented in Fig. 1a. According to Ostwald ripening mechanism, the small spheres are joined together and formed microsphere like structure during the hydrothermal processes. [P(VDF-HFP)] composites nanofibers containing PANI coated ZnS microsphere is prepared by using electrospinning method as shown in Fig. 1b [18]. The thickness of the fiber is 0.42 μm for all the samples of neat [P(VDF-HFP)] and its composite hybrid membrane.

3.1 Structural and morphological properties of PANI/ZnS composite

Figure 2a depicts the XRD- pattern of PANI coated ZnS microsphere. The XRD pattern of PANI/ZnS shows the diffraction peaks at 2θ values 14.4°, 20.5°, 25.3°, 28.6°, 48.2° and 57.3° are indexed to the (011), (020), (200), (111), (220) and (311) planes of PANI and ZnS phases, respectively [19, 20]. The XRD pattern for the PANI/ZnS composite shows that the prominent peaks correspond to the PANI and ZnS, these results confirmed that the presence of both ZnS and PANI in our samples. The elemental analysis (EDAX) spectra for PANI/ZnS composites is shown in Fig. 2b, in which the characteristic peaks of carbon (C), oxygen (O), zinc (Zn) and sulfide (S) peaks are found in the composite. Figure 2c shows the TEM images of the

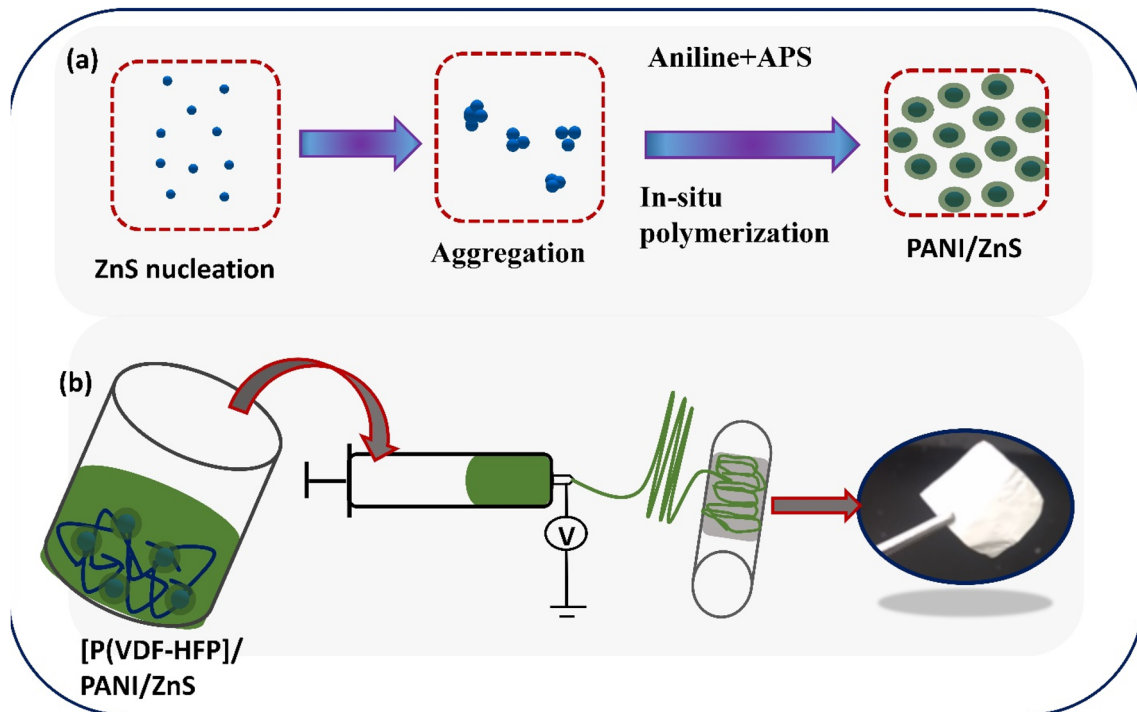


Fig. 1 a schematic representation of PANI coated ZnS microspheres, b schematic representation of the fabrication of electrospun nanofibers

PANI/ZnS composite. It looks like a core-shell structure with bright inner core and gray outer shell is observed for the PANI/ZnS composite. During the polymerization process, the aniline monomer begins to polymerize after the addition of APS, and then forms PANI layer on the ZnS surface. This is due to the electrostatic interactions of positively charged aniline and ZnS surface [21].

3.2 Structural properties of [P(VDF-HFP)]/PANI-ZnS composite nanofibers

The XRD patterns of the pure [P(VDF-HFP)] and its composite containing PANI, ZnS and PANI/ZnS microspheres are shown in Fig. 3a. The de-convoluted XRD plots shows the presence of electroactive β and γ -phases. As seen from the figure, the diffraction pattern of neat [P(VDF-HFP)] indexed at 2θ values 17.9° (100), 18.2° (020) and 19.8° (110) as the crystalline planes of the α -phase of the PVDF-HFP. The XRD pattern also indicates that with the loading of the PANI, ZnS and PANI/ZnS composite, the intensity of the α -phase became weak and another doublet diffraction peak appeared at $2\theta = 20.2^\circ$ corresponding to the reflection planes (110) and (200) attributed to the β and γ -phase [22, 23]. FTIR spectroscopy is

used to further calculate the content of the electroactive phases. The FTIR spectra (Fig. 3b) confirm the presence of α -phase in the PVDF-HFP films, which is evident from the 611, 764, 796, 974 and 1210 cm^{-1} bands [24]. The peaks at $1276, 841\text{ cm}^{-1}$ correspond to the β -phase [25].

Figure 3b reveals that the intensity of the α -phases in the case of composite fibers is decreased than in the case of the [P(VDF-HFP)] nanofibers and the β -phase is increased for the composite fibers. This is due to the interaction between the surface charges on the PANI/ZnS fillers and the CH_2/CF_2 dipoles of [P(VDF-HFP)] and thus increases the electroactive phase content of the composites [26]. Furthermore, the electroactive β -phase contents within the [P(VDF-HFP)] electrospun fibers can be calculated by the following formula [27].

$$F(\beta) = \frac{A_\beta}{1.26A_\alpha + A_\beta} \quad (1)$$

where A_β and A_α are the area of absorption bands at 841 and 764 cm^{-1} . The calculated values are shown in Fig. 3c, compared to the neat [P(VDF-HFP)], the content of β -phase is increased for the PANI, ZnS and PANI/ZnS composites.

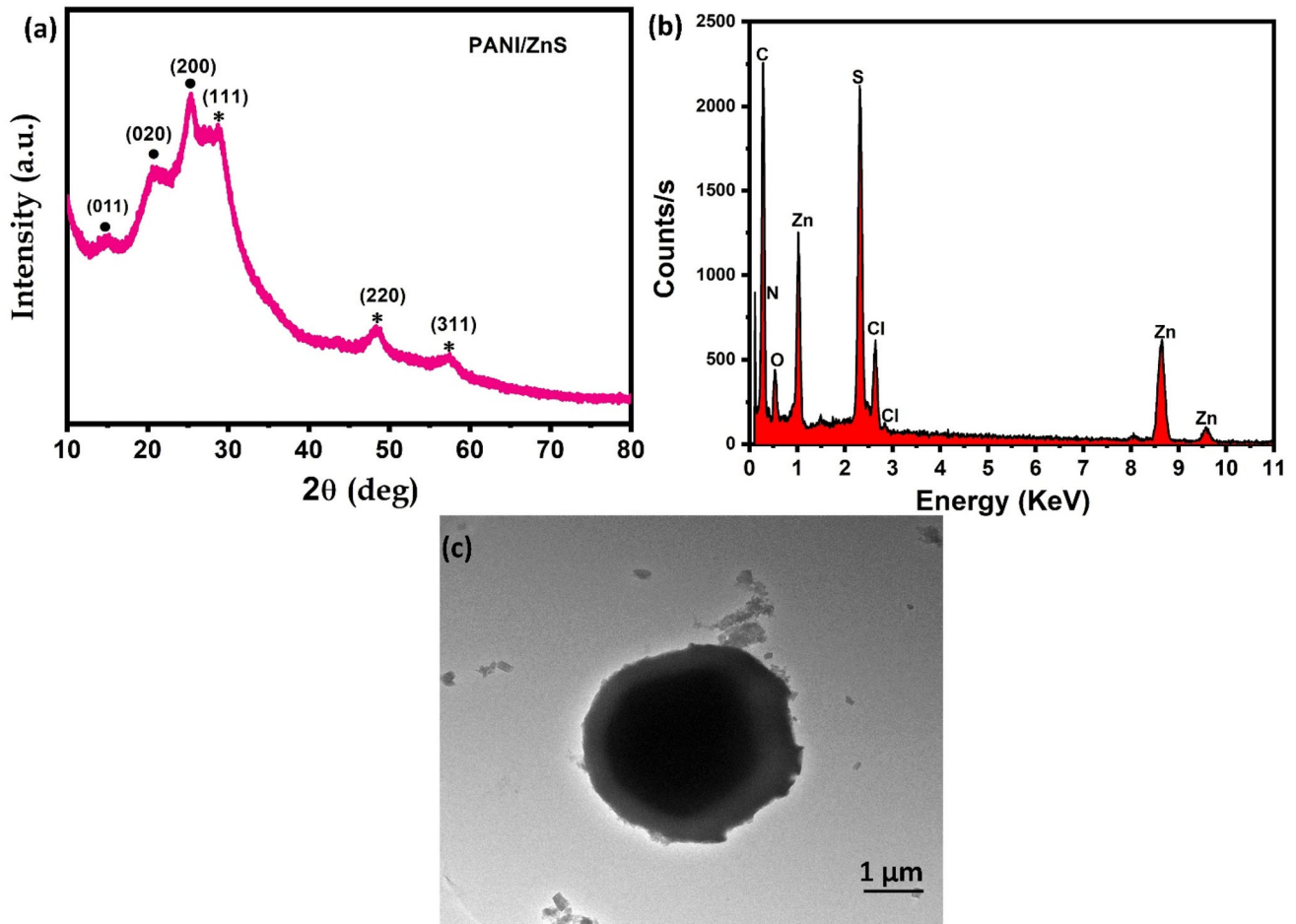


Fig. 2 a X-ray diffraction pattern of PANI coated ZnS microsphere [PANI, ZnS], b EDX spectrum for the PANI/ZnS, c TEM image of PANI/ZnS composite

3.3 Morphological properties of [P(VDF-HFP)]/PANI-ZnS composite nanofibers

Figure 4a–d show the morphological images of pure [P(VDF-HFP)] and its composite nanofibers.

The fiber diameter of the pure [P(VDF-HFP)] nanofiber is 600 nm and the fiber diameter is decreased for the composite nanofibers. A close look into Fig. 4d, the incorporation of PANI/ZnS microsphere significantly decreases the average diameter of composite nanofibers. It is found that an incorporation of PANI/ZnS composite caused the diameter of the fibers to decrease gradually from 600 to 280 nm. This is ascribed due to the increase in the conductivity of the solution in presence of the PANI/ZnS microspheres [28].

The increase in output performance of piezoelectric nanogenerator is mainly depends on the electroactive

β -phase The FTIR and XRD results show that the addition of PANI/ZnS particles in the [(PVDF-HFP)] matrix leads to an increase in electroactive β -phase nucleation. The reason for this β -phase enhancement is due to the electrostatic interaction between CH_2 or CF_2 dipoles of the [(PVDF-HFP)] chains and the surface charge of the PANI/ZnS.

The electrostatic interaction is described either as the interaction between the CH_2 dipoles in [P(VDF-HFP)] chains and negatively charged surfaces or as the interface between the CF_2 dipoles in [P(VDF-HFP)] chains and the positively charged surfaces [29]. The schematic diagram of proposed interfacial interaction between [(PVDF-HFP)] chains and the particle surface is presented in Fig. 5.

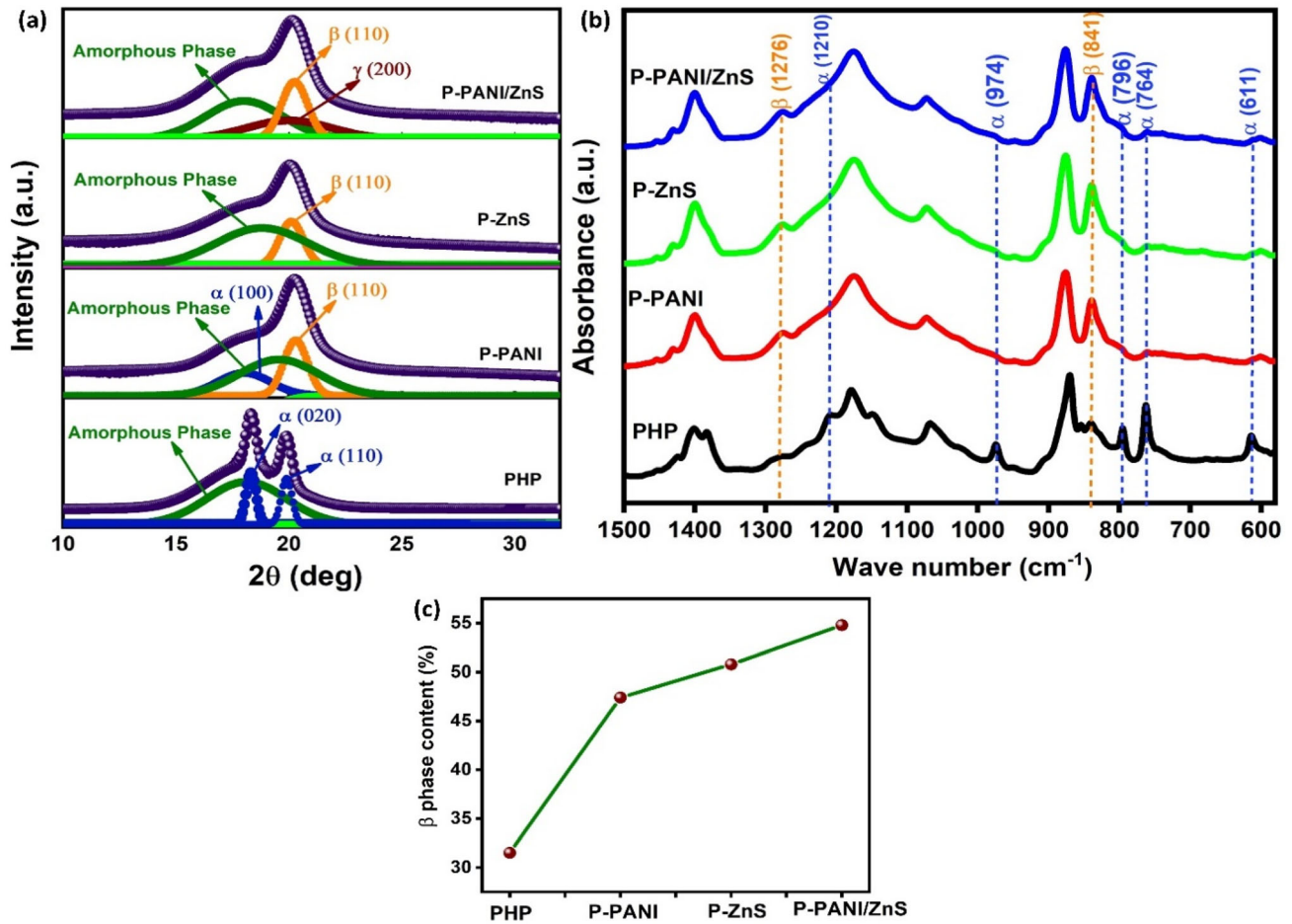


Fig. 3 **a** X-ray diffraction pattern of PVDF-HFP and its composites, **b** FTIR spectra of [(PVDF-HFP)] and its composite and **c** The calculated β -phase content in the composite

3.4 Mechanical properties of the composite nanofibers

The tensile stress-strain test that measures the elasticity of materials. The stress-strain curves of the sample is shown in Fig. 6a. For the tensile measurement, the nanofiber mats are carefully taken out from the aluminum sheet. The composite fiber mats exhibited highest stress and elongation at the breaking point. As shown in Fig. 6b, the elongation at the breaking point is increased for the PANI, ZnS and PANI/ZnS added composite fiber mats.

The improved mechanical properties of the composite nanofibers is due to the interaction of the PANI, ZnS and PANI/ZnS particles. The high mechanical properties of the composite nanofibers suggest that prepared electrospun nanofibers are more suitable for the fabrication of piezoelectric nanogenerator.

3.5 Dielectric properties of pure and the composite nanofibers

Figure 7 shows the dielectric constant and dielectric loss of the pure and [P(VDF-HFP)]/PANI-ZnS composite nanofibers. From Fig. 7a, the dielectric constant is increased for the composite nanofibers and it can attributed to the dispersion and conductive behavior of PANI/ZnS particles are the main reason for increasing dielectric constant. Also, the large accumulation of charge carriers at the interface between PANI/ZnS particles and [P(VDF-HFP)] chains leads to increase in dielectric constant. The high dielectric constant is due to the decrease in filler-filler distances and that promotes more dipole-dipole polarization in the composite nanofibers.

This high dipole polarization is responsible for the high output performance of the piezoelectric

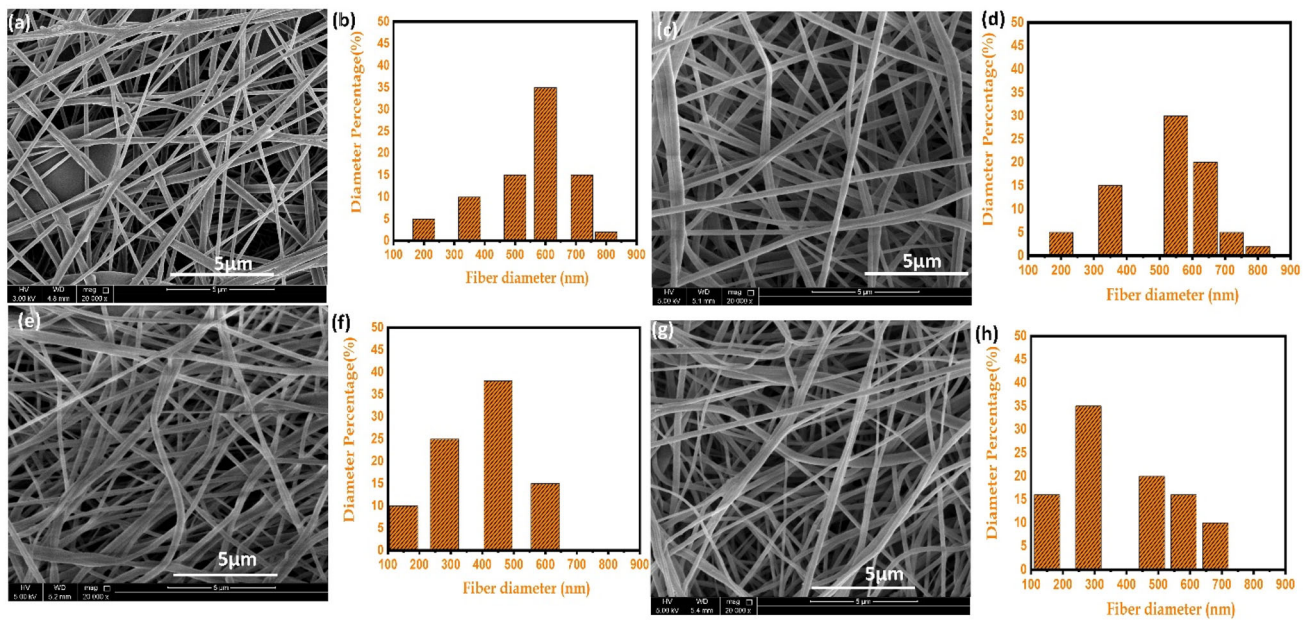


Fig. 4 SEM images and Fiber diameters of a, b pure PHP c, d P-PANI, e, f P-ZnS, g, h P-PANI/ZnS

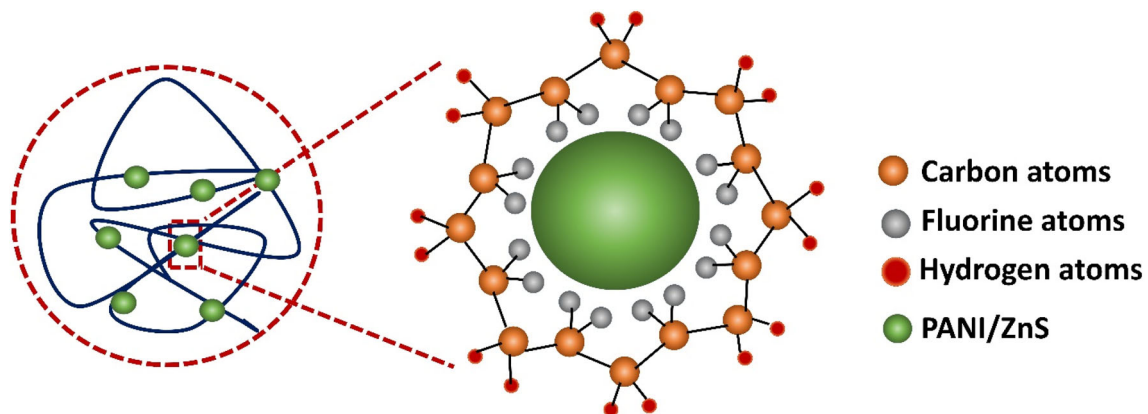


Fig. 5 Schematic diagram of the electrostatic interaction of the [P(VDF-HFP)] with PANI/ZnS microspheres composite for the formation of β -phase content in [P(VDF-HFP)]

nanogenerator. Which is more favorable for the piezoelectric potential development [30].

From Fig. 7b, it is also shown that the dielectric loss of the [P(VDF-HFP)]/PANI-ZnS composite nanofibers decreased compared with that of the neat [P(VDF-HFP)]. The decrease of leakage current is due to the fact that PANI reduced the mobility and concentration of ionizable hydroxyl groups on the surface of ZnS particles, resulting in the decrease of leakage current [31]. The improved dielectric constant and a low dielectric loss of [P(VDF-HFP)]/PANI-ZnS composites fibers could possibly find their application in energy storage devices.

3.6 Piezoelectric properties

To check the piezoelectric properties of the pure and PANI-ZnS/ [P(VDF-HFP)] composite nanofibers, flexible nanogenerators have been fabricated using carbon tape as an electrode and two wires were attached on both sides of the electrode. The piezoelectric output voltage is measured with the help of an assembled setup. Figure 8a, schematically illustrates the fabrication of piezoelectric nanogenerators. The flexibility of the nanogenerator is shown in Fig. 8b. The fabricated piezoelectric nanogenerator is tested for the piezoelectric performance by evaluating the output voltage. The sample is placed on the top of the

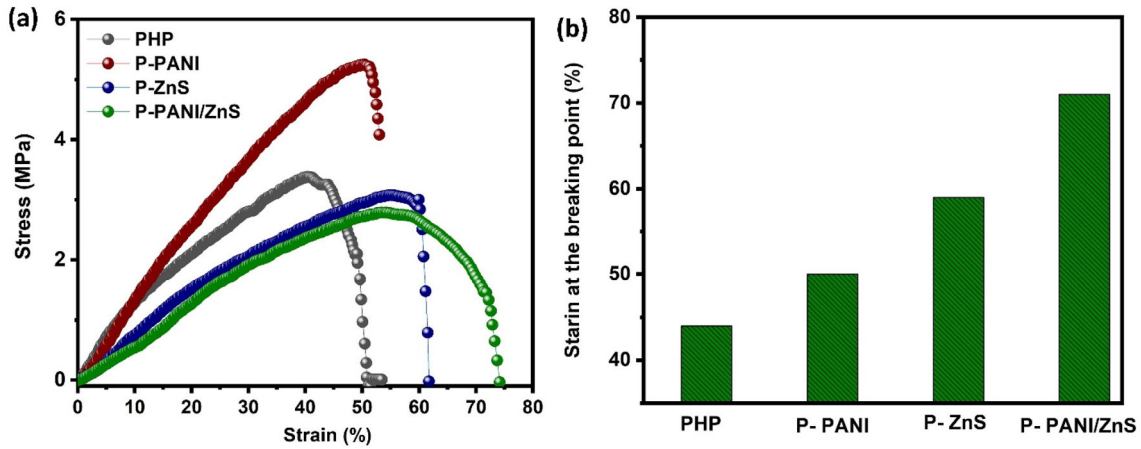


Fig. 6 a Stress-strain curves of the electrospun nanofibers, b Fracture strain of the nanofiber mats

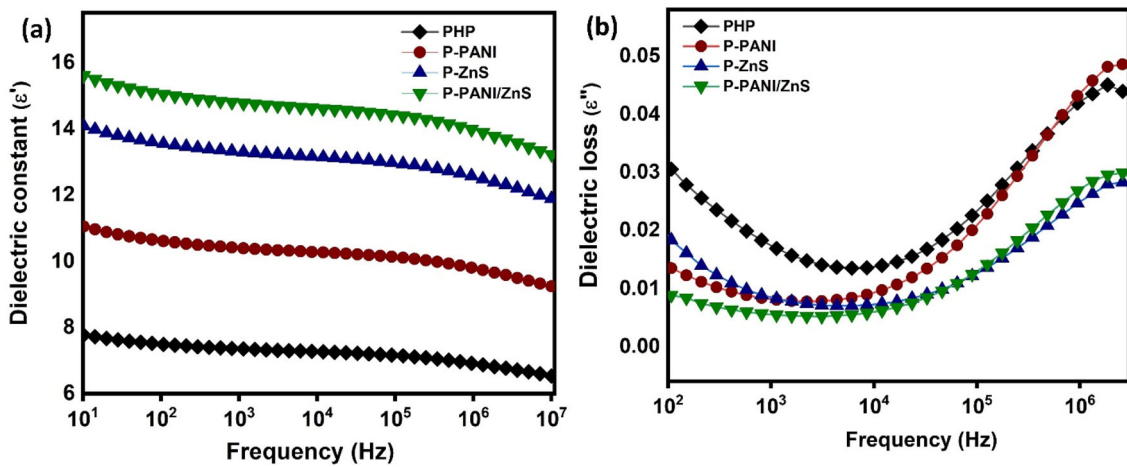


Fig. 7 a Frequency dependence of dielectric constant and b Frequency dependence of dielectric loss of composite nanofibers

vibrating shaker with a specific mass of 2.5 N. When the shaker vibrates, the mass will give compressive force on the material. The output voltage is measured by using data acquisition system. The output performance of the piezoelectric nanogenerator also depends on the frequency of applied force, because the mechanical energy from the ambient environment largely varies and is irregular. Bafri et al. [32] showed that 75 KHz frequency yielded 1.1 V output voltages. In this work, the samples were subjected to different frequencies ranging from 15 to 50 Hz, and the highest values obtained at 45 Hz. The maximum output voltages generated for all the samples at a specific vibration frequency (45 Hz). The sample details of the fabricated piezoelectric nanogenerator is shown in Table 1. Figure 8c–f shows the peak-peak output voltages for PHP, P-PANI, P- ZnS, P- PANI-ZnS composite nanofibers. The P-PANI-ZnS sample

showed a maximum peak-to-peak output voltage of 3 V (Fig. 8f). The large positive and negative peak is generated when the nanogenerator is subjected to imparting and releasing of the weight from the fabricated nanogenerator. Figure 8g shows the comparison of output voltage of the different composite nanofibers. When the external force is applied to the material, the composite nanofibers experienced a strain under a mechanical stress, which deformed the crystal structure of the composite nanofibers.

The presence of PANI/ZnS fillers in [P(VDF-HFP)] matrix generates a greater number of charges. This charge is easily transferred towards the electrodes through the PANI/ZnS conducting network. The high output performance of the composites nanofibers is due to the incorporation of core-shell PANI/ZnS microsphere. It acts as a nucleating agent and increases the β -phase of the neat [P(VDF-HFP)]

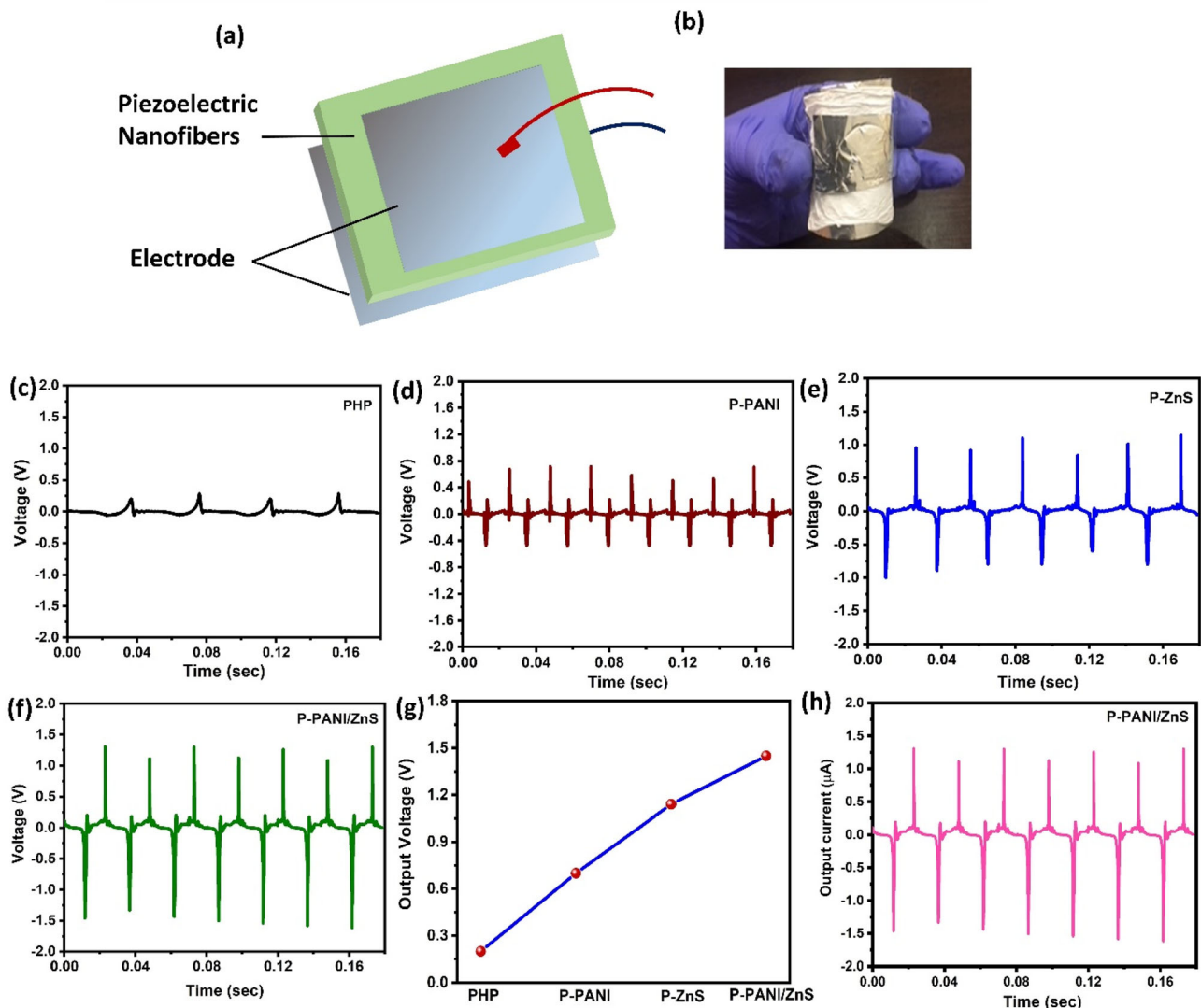


Fig. 8 **a** Schematics illustration of the piezoelectric nanogenerator fabrication, **b** Photographic images of the fabricated nanogenerator, **c–g** Output voltage as a function of time for the hybrid nanofibers

Table 1 The sample details of the fabricated PNG

Applied force	Types of electrodes	Frequency of excitation	Sample thickness	Output voltage
2.5 N	Electrospun fibers	45 Hz	0.42 μm	3 V

matrix. The internal carrier screening is reducing the piezoelectric output. In order to suppress the internal screening effect, the device is fabricated with core-shell structures. In our case, p-type PANI and n-type ZnS in composite formed a p-n heterojunction at the interface. The core-shell junction is important in suppressing the internal screening of the piezoelectric nanogenerator [33]. The core-shell composite increases the dielectric constant of the [P(VDF-HFP)]

matrix. Also, it enhances the self-polarization of the polymer matrix. The addition of PANI/ZnS core-shell structure acts as a conducting network between the piezoelectric materials. Therefore, the [P(VDF-HFP)]/2 wt% PANI-ZnS provides better output when compared to the neat polymer.

When no mechanical force is applied to the nanogenerator, there is no voltage peak is observed. When a mechanical stress is applied to the materials, the

Table 2 Comparison of piezoelectric performance of our system with other reported data

PVDF-based PNG with fillers	Poling voltage and duration	Output voltage	References
Graphene-titania-SrTiO ₃	6 kV for 7 s	2 V	[35]
Nanoclay	450 kV/cm for 30 min	3.5 V	[36]
BaTiO ₃ -h-BN	8 kV for 7 s	2.4 V	[37]
BaTiO ₃	150 MV/cm for 60 min	0.5 V	[38]
PANI-ZnS	Not required	3 V	Present work

piezoelectric output voltage is generated across the electrodes and free electrons will transfer across the electrodes. These free electrons will accumulate at the electrode nanofibers interface and create a output voltage. The instantaneous output power density follows the relation,

$$P = \frac{V^2}{A_{\text{eff}}XR_L} \quad (2)$$

where A_{eff} is the effective electrode area, V is the voltage and R_L load resistance [34]. Here the maximum power density obtained is $2.92 \mu\text{W}/\text{cm}^2$ for the composite nanofibers containing PANI-ZnS nanomaterials.

A Comparison of piezoelectric output performance of our material and literature reported piezoelectric nanogenerator is shown in Table 2. The piezoelectric performance of P(VDF-HFP)/PANI-ZnS is achieved simply using an electrospinning technique and exclusively produced a peak-to-peak output voltage of 3 V without applying any electrical poling. Compared with other system, P(VDF-HFP)/PANI-ZnS composite exhibits good output performance where electrical poling treatment is avoided.

4 Conclusions

In summary, we have fabricated flexible electrospun [P(VDF-HFP)]/2 wt% PANI/ZnS nanofibers for piezoelectric energy harvesting application. The electrospun nanofibers are prepared by using electrospinning technique. The synergistic effect of electrospinning and PANI/ZnS composite enhanced the content of the β -phase and interfacial polarization and it is confirmed from the XRD and FTIR technique. The piezoelectric output voltage is found to increase for the PANI/ZnS composite nanofibers. The fabricated piezoelectric nanogenerator generated a maximum peak-to-peak output voltage of 3 V. In

addition, the nanogenerator exhibited high dielectric constant and low dielectric loss, which is suitable for the energy storage devices. These results suggest that the fabricated flexible piezoelectric nanogenerator is suitable for energy harvesting system.

Acknowledgements

This work is supported by Qatar National Research Fund having project number UREP23-135-2-046. The findings achieved herein are solely the responsibility of the authors. The characterizations of this work are accomplished in the Central Laboratories unit, Qatar University. A part of the characterization has been accomplished in the Gas Processing Center, College of Engineering Qatar University.

Funding

Open access funding provided by the Qatar National Library.

Open Access This article is licensed under a Creative Commons Attribution 4.0 International License, which permits use, sharing, adaptation, distribution and reproduction in any medium or format, as long as you give appropriate credit to the original author(s) and the source, provide a link to the Creative Commons licence, and indicate if changes were made. The images or other third party material in this article are included in the article's Creative Commons licence, unless indicated otherwise in a credit line to the material. If material is not included in the article's Creative Commons licence and your intended use is not permitted by statutory regulation or exceeds the permitted use, you will need to obtain permission directly from the copyright holder. To view a copy of

this licence, visit <http://creativecommons.org/licenses/by/4.0/>.

Supplementary Information: The online version of this article (<https://doi.org/10.1007/s10854-021-05352-4>) contains supplementary material, which is available to authorized users.

References

- Z.L. Wang, J. Song, *Science*. **312**, 242–246 (2006)
- C. Dagdeviren, Z. Li, Z.L. Wang, *Annu.Rev. Biomed. Eng.* **19**, 85–108 (2017)
- X. Chen, S. Xu, N. Yao, Y. Shi, *Nano Lett.* **10**(6), 2133–2137 (2010)
- K.-I. Park, S. Xu, Y. Liu, G.-T. Hwang, S.-J.L. Kang, Z.L. Wang, K.J. Lee, *Nano Lett.* **10**(12), 4939–4943 (2010)
- A. Sultana, M.M. Alam, S. Garain, T.K. Sinha, T.R. Middy, D. Mandal, *ACS Appl. Mater. Interfaces*. **7**(34), 19091–19097 (2015)
- T.K. Sinha, S.K. Ghosh, R. Maiti, S. Jana, B. Adhikari, D. Mandal, S.K. Ray, *ACS Appl. Mater. Interfaces*. **8**(24), 14986–14933 (2016)
- S. Nayak, T. Kumar Chaki, D. Khastgir, *Advanced Materials Research, Trans Tech Publ.* (2013), pp. 897–900
- G. Shen, Y. Bando, J. Hu, D. Golberg, *Appl. Phys. Lett.* **90**(12), 123101 (2007)
- Y. Cheng, C. Jin, F. Gao, X. Wu, W. Zhong, S. Li, P.K. Chu, *J. Appl. Phys.* **106**(12), 123505 (2009)
- L. Chen, M.-C. Wong, G. Bai, W. Jie, J. Hao, *Nano Energy*. **14**, 372–381 (2015)
- C. Chang, V.H. Tran, J. Wang, Y.-K. Fuh, L. Lin, *Nano Lett.* **10**(2), 726–731 (2010)
- M. Khalifa, S. Anandhan, *ACS Appl. Nano Mater.* **2**(11), 7328–7339 (2019)
- X.-J. Zhang, G.-S. Wang, Y.-Z. Wei, L. Guo, M.-S. Cao, *J. Mater. Chem. A*. **1**(39), 12115–12122 (2013)
- F. Mokhtari, M. Shamshirsaz, M. Latifi, S. Asadi, *J. Text. Inst.* **108**(6), 906–914 (2017)
- B. Li, F. Zhang, S. Guan, J. Zheng, C. Xu, *J. Mater. Chem. C*. **4**(29), 6988–6995 (2016)
- L. Persano, C. Dagdeviren, Y. Su, Y. Zhang, S. Girardo, D. Pisignano, Y. Huang, J.A. Rogers, *Nat. Commun* **4**(1), 1–10 (2013)
- H. Parangusan, D. Ponnamma, M.A.A. AlMaadeed, *RSC Adv.* **7**(79), 50156–50165 (2017)
- D. Ponnamma, H. Parangusan, A. Tanvir, M.A.A. AlMaadeed, *Mater. Des.* **184**, 108176 (2019)
- D. Gui, C. Liu, F. Chen, J. Liu, *Appl. Surf. Sci.* **307**, 172–177 (2014)
- Y.-C. Liang, S.-L. Liu, *Nanoscale Res. Lett.* **9**(1), 1–7 (2014)
- B. Sim, H. Chae, H. Choi, *Express Polym. Lett.* **9**(8) (2015)
- P. Adhikary, A. Biswas, D. Mandal, *Nanotechnology*. **27**(49), 495501 (2016)
- B. Neese, Y. Wang, B. Chu, K. Ren, S. Liu, Q. Zhang, C. Huang, J. West, *Appl. Phys. Lett.* **90**(24), 242917 (2007)
- P. Adhikary, D. Mandal, *Phys. Chem. Chem. Phys.* **19**(27), 17789–17798 (2017)
- S. Manna, A.K. Nandi, *J. Phys. Chem. B.* **115**(42), 12325–12326 (2011)
- D. Mandal, K. Henkel, D. Schmeißer, 2011 International Conference on Nanoscience, Technology and Societal Implications, IEEE, 2011, pp. 1–5
- L. Li, M. Zhang, M. Rong, W. Ruan, *RSC Adv.* **4**(8), 3938–3943 (2014)
- M.M. Alam, S.K. Ghosh, A. Sultana, D. Mandal, *ACS Sustain. Chem. Eng.* **6**(1), 292–299 (2018)
- H. Parangusan, D. Ponnamma, M.A.A. AlMaadeed, *ACS omega*. **4**(4), 6312–6323 (2019)
- K.Y. Lee, D. Kim, J.H. Lee, T.Y. Kim, M.K. Gupta, S.W. Kim, *Adv. Funct. Mater.* **24**(1), 37–43 (2014)
- B. Luo, X. Wang, Y. Wang, L. Li, *J. Mater. Chem. A*. **2**(2), 510–519 (2014)
- M.S.S. Bafqi, R. Bagherzadeh, M. Latifi, *J. Polym. Res.* **22**(7), 130 (2015)
- A. Waseem, M.A. Johar, M.A. Hassan, I.V. Bagal, J.-S. Ha, J.K. Lee, S.-W. Ryu, *Nano Energy*. **60**, 413–423 (2019)
- H. Parangusan, D. Ponnamma, M.A.A. AlMaadeed, *Soft Matter*. **14**(43), 8803–8813 (2018)
- D. Ponnamma, A. Erturk, H. Parangusan, K. Deshmukh, M.B. Ahamed, M.A.A. Al-Maadeed, *Emergent Materials*. **1**(1–2), 55–65 (2018)
- A. Gaur, R. Shukla, B. Kumar, A. Pal, S. Chatterji, R. Ranjan, P. Maiti, *Polymer*. **97**, 362–369 (2016)
- D. Ponnamma, M.A.A. Al-Maadeed, *Sustain Energy Fuels* **3**(3), 774–785 (2019)
- J. Nunes-Pereira, V. Sencadas, V. Correia, V.F. Cardoso, W. Han, J.G. Rocha, S. Lanceros-Méndez, *Compos. B. Eng.* **72**, 130–136 (2015)

Publisher's note Springer Nature remains neutral with regard to jurisdictional claims in published maps and institutional affiliations.